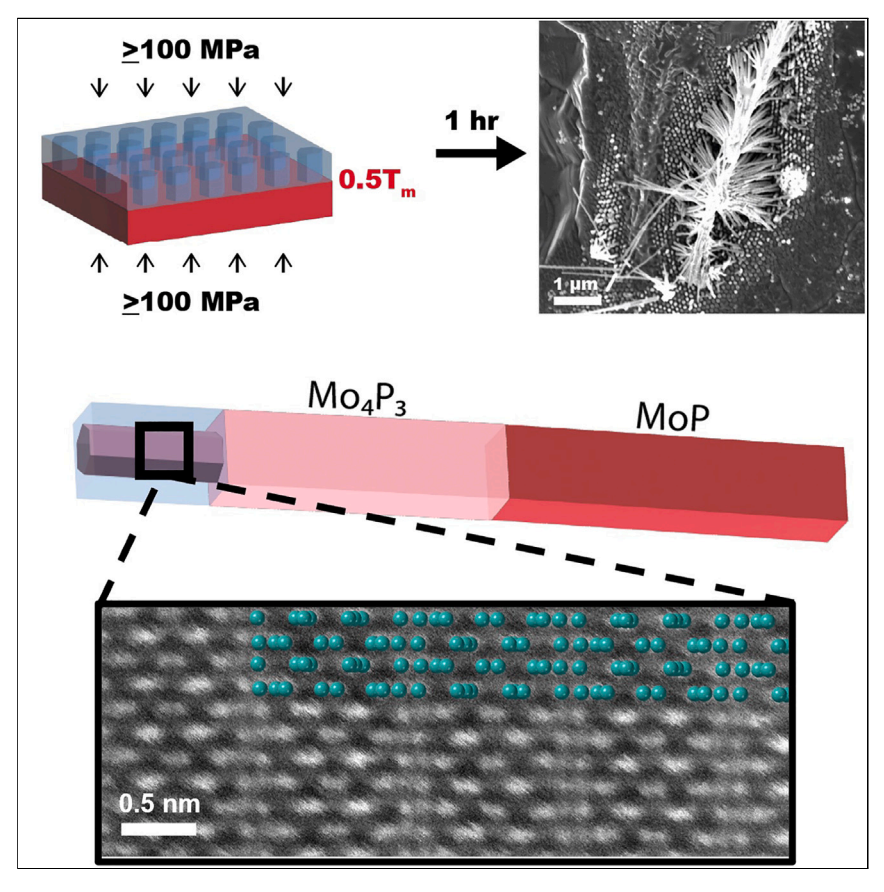
Matter



Article

Nanomolding of metastable Mo₄P₃



Fabricating materials that are not stable at room temperature gives scientists a larger materials toolbox to choose from. We detail a new approach to making metastable materials at the nanoscale by pressing a bulk feedstock at moderate temperatures through a nanoporous mold. By "nanomolding" MoP, the resulting nanowires become $\mathrm{Mo_4P_3}$, a material that is not typically stable at room temperature. This approach can be extended to numerous other compounds that have ideal electronic, optical, and catalytic properties.

Mehrdad T. Kiani, Quynh P. Sam, Gangtae Jin, ..., James L. Hart, J.R. Stauff, Judy J. Cha

jc476@cornell.edu

Highlights

Large-scale nanomolding of nanowires of covalently bonded compounds

Synthesis of metastable phase inaccessible at ambient pressure

Electronic property characterization of Mo₄P₃ nanowires



Matter



Article

Nanomolding of metastable Mo₄P₃

Mehrdad T. Kiani,¹ Quynh P. Sam,¹ Gangtae Jin,¹ Betül Pamuk,² Hyeuk Jin Han,^{1,3} James L. Hart,¹ J.R. Stauff,⁴ and Judy J. Cha^{1,5,*}

SUMMARY

Reduced dimensionality leads to emergent phenomena in quantum materials, and there is a need for accelerated materials discovery of nanoscale quantum materials in reduced dimensions. Thermomechanical nanomolding is a rapid synthesis method that produces high-quality single-crystalline nanowires with controlled dimensions over wafer-scale sizes. Herein, we apply nanomolding to fabricate nanowires from bulk feedstock of MoP, a triple-point topological metal with extremely high conductivity that is promising for low-resistance interconnects. Surprisingly, we obtained singlecrystalline Mo₄P₃ nanowires, which is a metastable phase at room temperature and atmospheric pressure. We thus demonstrate that nanomolding can create metastable phases inaccessible by other nanomaterial syntheses and can explore a previously inaccessible synthesis space at high temperatures and pressures. Furthermore, our results suggest that the current understanding of interfacial solid diffusion for nanomolding is incomplete, providing opportunities to explore solid-state diffusion at highpressure and high-temperature regimes in confined dimensions.

INTRODUCTION

1D material systems display emergent phenomena due to reduced dimensionality and nanoscale confinement not present in higher dimensions, such as dislocation starvation in nanopillars, deviations in crystallization in metallic glasses, and ballistic transport in 1D van der Waals crystals. In the context of quantum materials, realizing topological superconductors for probing Majorana bound states, maximizing topological surface states for low-dissipation microelectronics or catalysis, and developing Josephson junctions with unusual current-phase relations all rely on pristine 1D nanowire systems. Given the large predicted number of topological quantum materials, there are limited nanofabrication techniques that allow for simultaneous morphological, crystallographic, and structural control of 1D nanowires over wafer-scale distances. Traditional bottom-up fabrication techniques such as chemical vapor deposition or molecular beam epitaxy require extensive optimization, and yet control of size and defect structure is limited, while top-down lithographic approaches can achieve the desired size but lack any control of defect structure and are severely limited with respect to material choice.

In 2019, Liu et al. introduced the scalable fabrication method of thermomechanical nanomolding (TMNM), where a bulk polycrystalline feedstock material is extruded through a nanoporous mold at elevated temperatures (approximately $0.5T_m$, where T_m is the melting point) and pressures (>100 MPa). This process results in the formation of single-crystalline, defect-free nanowires with high aspect ratios. The mold is etched away using a strong acid or base, and the molded nanowires are

PROGRESS AND POTENTIAL

Large-scale manufacturing of nanostructures with controlled morphology and high crystalline quality can be transformative for many applications, such as sensing, catalysis, plasmonic, and electronic applications, but remains challenging. Thermomechanical nanomolding has recently been developed to fabricate large-scale nanowires of metals and intermetallics with controlled diameter and aspect ratios. This work extends the capability of nanomolding and demonstrates controlled and scalable nanomolding of singlecrystalline Mo₄P₃, which is a metastable phase at room temperature at ambient pressure. Thus, we demonstrate thermomechanical nanomolding as a scalable nanofabrication technique for metastable compounds as well as quantum materials.





separated from the bulk feedstock via sonication. TMNM holds several key advantages over traditional synthesis methods, including the ability to produce single-crystalline nanostructures from a polycrystalline feedstock due to reorientation of the grains as they are pressed through the mold. 12 Another major advantage of TMNM is its versatility, as the library of successfully nanomolded materials has expanded to include crystalline metals, 13 solid solutions, 10 and ordered phases.1

The use of TMNM for 1D quantum materials has been unexplored. One particular issue is that many quantum materials of interest possess covalent bonding, such as metal phosphides.^{15–18} Molybdenum phosphides such as MoP, ^{16,19} MoP₂, ^{17,20} and MoP₄¹⁵ exhibit unique quantum transport effects arising from topologically protected surface states, and MoP, a triple-point topological metal,²¹ is a promising alternative to Cu as a low-resistance interconnect due to its high carrier density, high electron mobility, and low bulk resistivity. In Mo-P compounds, metallic bonding exists between Mo atoms; however, the shortest atomic bond distances are between covalently bonded Mo and P atoms.²² Previous TMNM studies focused on metals or intermetallics with largely metallic bonding, 13,14 which can make bond rearrangement during solid-state diffusion easier, while certain covalently bonded materials such as Si are not suitable for TMNM given their extremely low bulk and surface diffusivities. 14

We herein report the nanomolding of single-crystalline nanowires from a polycrystalline MoP feedstock. Surprisingly, crystallographic and compositional analysis shows the nanowires to be Mo_4P_3 instead of MoP. Mo_4P_3 is a metastable phase at room temperature and ambient pressure with little experimental characterization. Density functional theory (DFT) band structure calculations and resistivity measurements indicate that Mo₄P₃ is a non-topological metal with resistivity values comparable to other molybdenum-phosphide compounds. These results demonstrate that high temperatures and pressures, along with the interfacial energy between the feedstock and mold materials in TMNM, can provide a novel pathway to nanofabrication of metastable phases.

RESULTS AND DISCUSSION

Bulk polycrystalline MoP, which has been polished to a mirror finish, is used as the initial feedstock material (Figure S1). TMNM is performed at 1000°C and 150 MPa for 3 h using an anodic aluminum oxide (AAO) mold with 40 nm pores (Figures 1A and 1B) in an argon environment. Etching of the mold in hydrofluoric acid (HF) and sonication lead to dispersed nanowires in solution (Figures 1C and 1D), which are drop cast onto transmission electron microscopy (TEM) grids or SiO₂ substrates for characterization and electrical measurements, respectively. Details of TMNM can be found in the supplemental information.

Scanning TEM (STEM) is used to characterize the molded nanowires. The average diameter of the nanowires is 33.8 \pm 1.9 nm. High-angle annular dark field (HAADF) STEM images reveal that the nanowires have a different atomic structure from their bulk MoP feedstock (Figure S1). The high-resolution STEM image in Figure 2D shows that the atomic structure of the nanowires is not the hexagonal crystal structure of MoP or MoP₂, shown in Figure S2. From crystallographic analysis, we determine the phase of the nanowires to be orthorhombic Mo₄P₃ (Figures 2A and 2B), a high-temperature compound stable between 700°C and 1,580°C at ambient pressure.²³ As shown by the overlay in Figure 2D, the atomic positions in the STEM

¹Department of Materials Science and Engineering, Cornell University, Ithaca, NY 14853,

²School of Applied and Engineering Physics, Cornell University, Ithaca, NY 14853, USA

³Department of Environment and Energy Engineering, Sungshin Women's University, Seoul 01133, South Korea

⁴Department of Mechanical Engineering and Materials Science, Yale University, New Haven, CT 06520, USA

⁵Lead contact

^{*}Correspondence: ic476@cornell.edu https://doi.org/10.1016/j.matt.2023.03.023





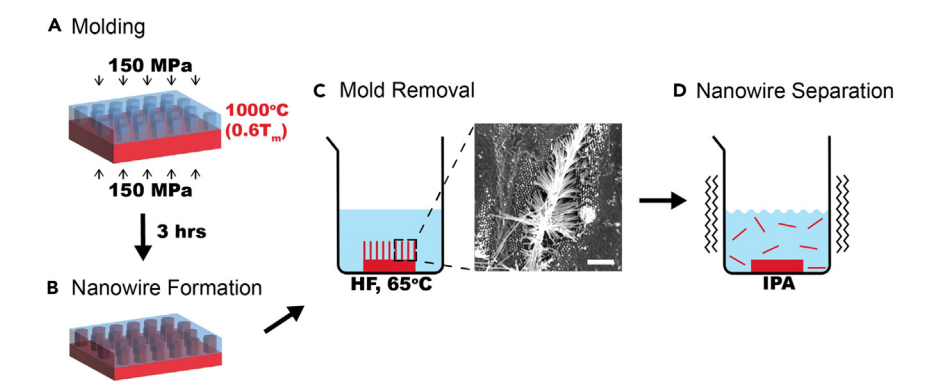


Figure 1. Schematic of the TMNM process

- (A) Molding of polycrystalline MoP feedstock (red) using an anodic aluminum oxide mold (blue) at high temperature and pressure.
- (B) Formation of single-crystalline nanowires after a mold period of 3 h.
- (C) Mold removal using hydrofluoric acid (HF) and scanning electron microscope (SEM) image of nanowires molded from MoP feedstock (scale bar: $1~\mu m$).
- (D) Separation of nanowires from feedstock via sonication in isopropyl alcohol (IPA).

image closely match those of the Mo atoms in Mo_4P_3 , with the growth direction along the b axis. The lattice constant perpendicular to the growth direction of the nanowire is measured to be 21.3 Å, which nearly matches the Mo_4P_3 c lattice constant of 20.5 Å.²⁴ The 3.9% discrepancy can be attributed to tensile strain along the curvature of the nanowire. Using the fast Fourier transform (FFT) of the STEM image, shown in Figure S3, we calculate the lattice constant along the growth direction of the nanowire to be 3.2 Å, in close agreement with the b lattice constant of Mo_4P_3 of 3.16 Å.²⁴ Figure 2E shows the normalized energy-dispersive X-ray spectroscopy (EDX) spectrum of the molded nanowires compared with two reference spectra measured from bulk single crystals of MoP and MoP_2 . Using the reference spectra, the Mo-to-P ratio of the nanowires is calculated to be nearly 4:3 (Table S1). STEM-EDX maps (Figure S4) show that the distribution of Mo and P is uniform over the entire area of the nanowires. No Mo_4P_3 nanowire had noticeable oxide formation; however, some had residual AAO mold.

Diffraction data are collected via 4D STEM scan over the nanowire shown in Figure 2C to confirm its single-crystalline nature. Figure 2F shows a diffraction pattern generated by summing up the 4D STEM data over an area of 726 nm^2 on the nanowire outlined in Figure S5. The diffraction pattern shows that the nanowire is single crystalline and a close qualitative match to the simulated diffraction pattern of Mo_4P_3 shown in Figure 2G. The area of integration for the diffraction pattern was limited to avoid shifts in the diffraction spots arising from changes in nanowire orientation on the TEM grid due to bending, which would distort the final diffraction pattern. In Figure 2H, single diffraction patterns taken from different points along the wire length confirm that the nanowire is single crystalline, unlike the starting bulk polycrystalline MoP (Figure S1). While there are changes in the intensity of the diffraction spots due to varying orientations along the length of the nanowire, the overall diffraction spot positions remain consistent owing to the lack of grains.

The present work shows that crystal structure and composition can change during nanomolding to stabilize and produce metastable Mo_4P_3 nanowires from the bulk feedstock of MoP. This observation is distinct from previous nanomolding

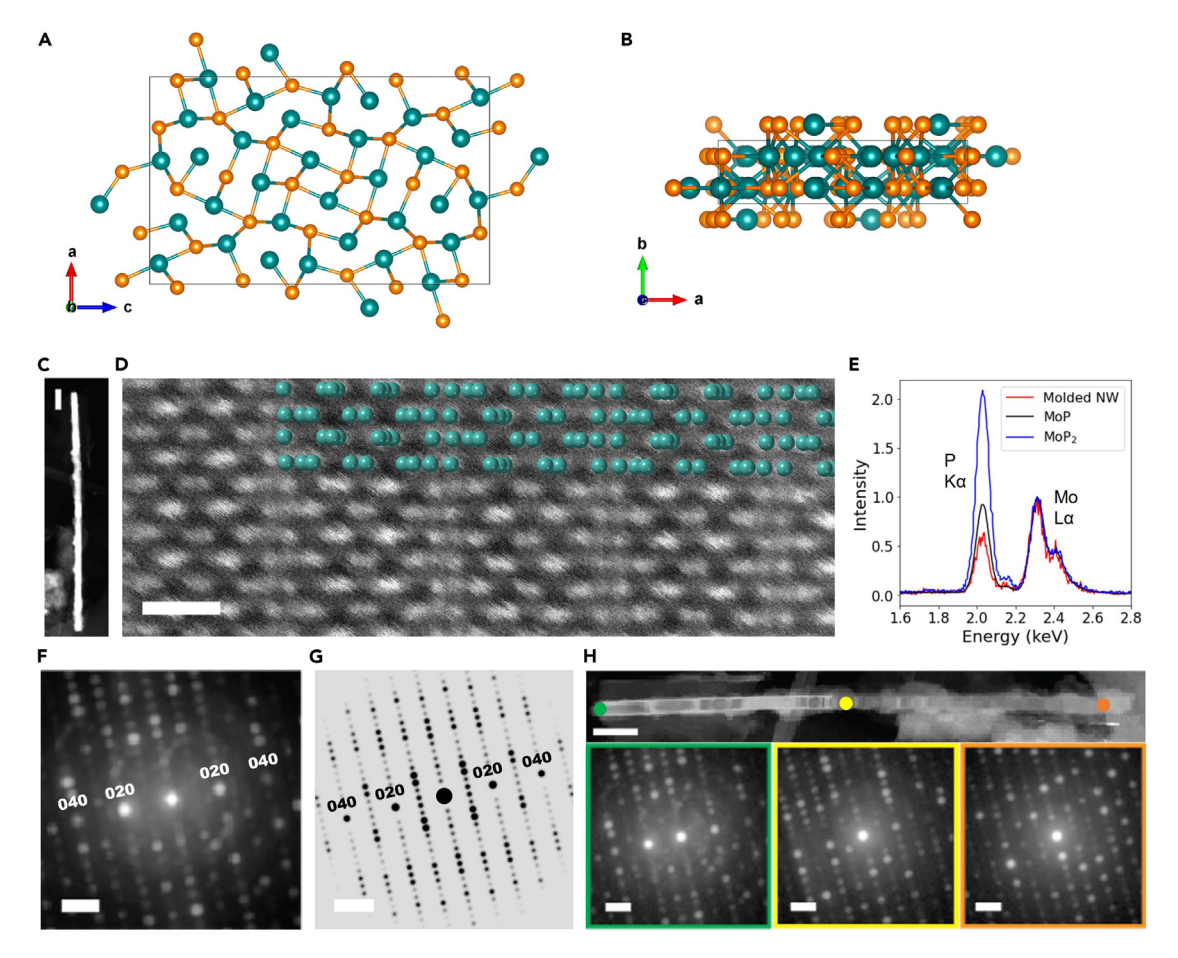


Figure 2. Atomic characterization of molded nanowires

(A and B) Schematics of $\mathrm{Mo_4P_3}$ crystal structure (Mo atoms in teal, P atoms in orange).

- (C) Low-magnification image of nanowire (scale bar: 0.1 µm).
- (D) STEM image of nanowire (scale bar: 5 Å).
- (E) EDX spectra of molded nanowire, reference MoP, and MoP_2 bulk single crystals.
- (F) Integrated diffraction pattern over 6 \times 6 pixel area of nanowire from 4D STEM (scale bar: 0.5 Å⁻¹).
- (G) Simulated diffraction pattern of Mo_4P_3 (scale bar: 0.5 $\mbox{\normalfont\AA}^{-1}$).
- (H) Diffraction patterns (scale bar: $0.5~\text{Å}^{-1}$) from three points along the length of the nanowire (scale bar: $0.1~\mu m$).

experiments, where chemical composition and crystal structure of the molded nanowires matched the bulk feedstock. ¹⁴ We propose two potential mechanisms that could lead to loss of phosphorus during molding. Due to the high temperatures involved during molding and the high vapor pressure of phosphorus compared with molybdenum, ²⁵ the nanowires could slowly lose phosphorus during molding, leading to a change in chemical composition and crystal structure. Alternatively, phosphorus could be diffusing into the AAO mold, as alumina has a strong binding affinity for phosphates, ²⁶ and lateral diffusion of phosphorus from the wires into the AAO could lead to a change in composition and crystal structure in the nanowires during molding.

To determine the cause of phosphorus loss during nanomolding, we performed STEM-EDX mapping on the Mo_4P_3 nanowires still embedded in unetched, intact AAO mold that is in contact with the bulk feedstock, prepared by focused ion beam (FIB) milling. STEM-EDX of the FIB-prepared sample (Figure 3A) shows no Mo or P in the AAO mold. Instead, the P/Mo EDX peak ratio along the molding

Matter Article



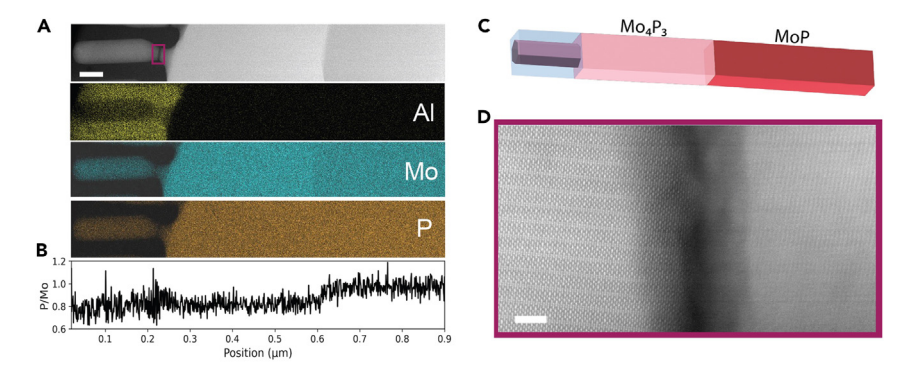


Figure 3. Conversion from MoP to Mo₄P₃ during molding

- (A) STEM-EDX map of Mo₄P₃ nanowire FIB liftout with AAO mold. Scale bar: 50 nm.
- (B) P-K α /Mo-L α EDS peak ratio along the scan region.
- (C) Schematic of the nanomolding region with different crystal structures.
- (D) STEM image showing crystal rotation near entrance of nanowire into AAO mold from (A). Scale bar: 2 nm.

direction (Figure 3B) shows that the phosphorus content has decreased in the nanowire as well as the first \sim 400 nm of the bulk feedstock. Thus, we determine that phosphorus atoms are not diffusing into the AAO mold during molding. Rather, due to the high vapor pressure of phosphorus²⁵ at the molding temperature, the MoP bulk feedstock near the surface of the AAO mold is losing phosphorus and converting to Mo₄P₃ during nanomolding. Phosphorus is able to leave the bulk feedstock through the pores in the AAO mold and the gaps between the mold and feedstock due to surface roughness. We note that only the first \sim 400 nm of the bulk feedstock near the surface is converted to Mo₄P₃, while the rest of the feedstock remains MoP (Figure 3C). This can also be inferred in the HAADF-STEM image shown in Figure 3A, where the first 400 nm of the bulk feedstock is brighter in intensity with a clear boundary that separates the Mo₄P₃ region from the MoP region. Therefore, Mo₄P₃ nanowires are formed from the locally converted Mo₄P₃ feedstock during molding. Interestingly, the Mo₄P₃ nanowire shows a drastic change in crystalline orientation from the bulk Mo₄P₃ (Figure 3D), which occurs in order to minimize the overall surface energy of the nanowire, in agreement with previous molding results on nanomolding. 12,13

As MoP, 16,19 MoP₂, 17,20 and MoP₄ 15 possess topologically protected electronic states, it might be the case that Mo_4P_3 is also topological. However, there are limited computational and experimental studies on transport properties of bulk Mo₄P₃ since it is a metastable phase not found at room temperature. Shirotani et al. found that bulk Mo₄P₃ prepared under high pressure exhibits superconductivity at 3 K,²² but they do not measure room temperature resistivity. The electronic band structure calculated from DFT (Figure 4A) reveals that Mo₄P₃ is metallic. Orbitally projected band structures do not present any band crossings with a parity change from Mo d states to P p states (Figure 4A), with mainly Mo d orbitals contributing to bands down to -2 eV relative to the Fermi level (Figures 4A and S6). Therefore, Mo₄P₃ is unlikely to be topological. The total density of states (Figure S6) is comparable to other Mo-P intermetallic compounds.²⁷ The growth direction of the molded nanowires, and subsequently the direction of current flow, is along the b axis, which corresponds to the Γ -Y direction in the band structure (Figure 4B). To measure resistivity, we fabricated four-point probes on Mo₄P₃ nanowires deposited on SiO₂ using e-beam-deposited Ti/Au electrodes (Figure 4C). From four-point probe



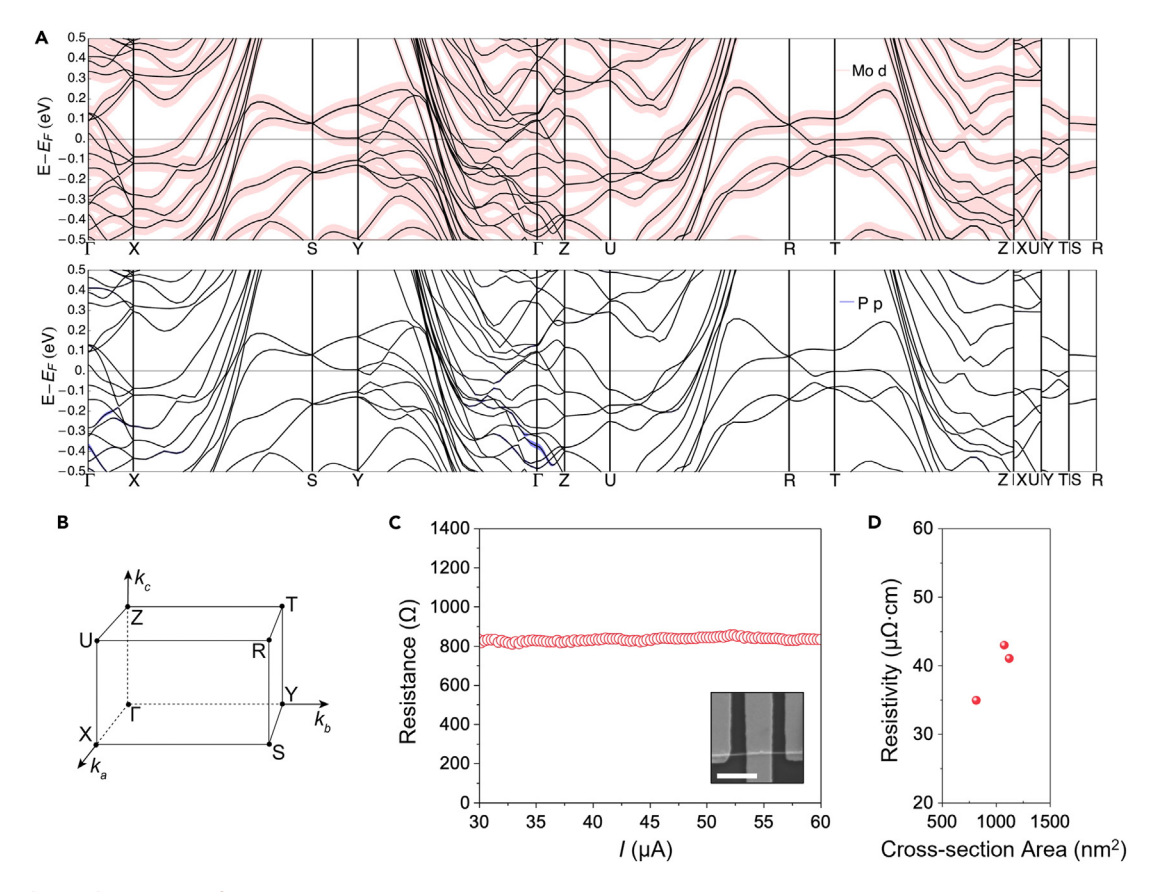


Figure 4. Electrical properties of $\mathrm{Mo_4P_3}$

- (A) Calculated orbitally projected band structure of Mo d (red) and P p (blue) states near Fermi level for Mo₄P₃.
- (B) High symmetry labels for Brillouin zone of Mo_4P_3 .
- (C) Resistance versus current of Mo_4P_3 nanowire during four-point probe measurement. Inset is SEM image of four-point probe with a scale bar of 1 μm .
- (D) Resistivity of Mo_4P_3 nanowires with differing cross-sectional area.

measurements, the resistivity of the Mo $_4$ P $_3$ nanowires is measured to be 39.7 \pm 3.4 $\mu\Omega$ •cm at 300 K (Figure 4D). Since no experimental resistivity values exist for bulk or nanostructure Mo $_4$ P $_3$, we compare the resistivity with *ab initio* calculations, which report a range from 3.3 to 33 $\mu\Omega$ •cm (Tables S2 and S3). Since the resistivity values of Mo $_4$ P $_3$ nanowires are comparable to the predicted bulk value, we hypothesize that surface electron scattering is minimal. The resistivity value of the Mo $_4$ P $_3$ nanowires measured is higher than that of MoP nanowires, 29 12 $\mu\Omega$ •cm, for the equivalent cross-sectional area but is comparable to single-crystal 60 nm diameter MoP $_2$ nanowires 20 (32 $\mu\Omega$ •cm).

In conclusion, we show that TMNM is a viable nanofabrication strategy for 1D quantum materials. Using a bulk MoP feedstock, we nanomold Mo_4P_3 nanowires and confirm their single-crystalline, defect-free structure. To date, this is the only nanofabrication technique for single-crystal 1D nanowires for Mo_4P_3 and the first demonstration of TMNM for a largely covalently bonded material. DFT calculations showed a non-topological metallic character for Mo_4P_3 , and resistivity values of nanowires are comparable to other molybdenum phosphides and close to predicted bulk resistivity, indicating that surface scattering is minimal. Since TMNM is material agnostic, the approach elucidated here can be extended to fabricate other metastable metal phosphides or covalently bonded systems.

Matter Article



EXPERIMENTAL PROCEDURES

Resource availability

Lead contact

Further information and requests for resources and materials should be directed to and will be fulfilled by the lead contact, Judy J. Cha (jc476@cornell.edu).

Materials availability

Nanowires of Mo_4P_3 can be requested; contact the lead contact.

Data and code availability

This study did not generate or analyze datasets or code.

Bulk MoP feedstock fabrication

MoP powder (Alfa Aesar) was loaded into a graphite die, then pressed and heated at 150 MPa and 900°C for 3 h. The pellet was removed from the die and sintered at 1,000°C overnight in 5% H_2 in Ar. XRD measurements were taken on the pellet prior to and after sintering to verify the MoP phase (Figure S1). The pellet was cut into smaller pieces and polished for molding.

Nanowire fabrication

AAO molds with 40 nm pore size and 50 μ m thickness were purchased from InRedox. A cut and mirror-polished piece of the MoP pellet was placed on an AAO mold in a graphite die. After heating to 1,000°C at 10 °C/min under argon, the sample was loaded to 150 MPa for 3 h. After allowing the pressed sample to cool to room temperature, the AAO mold was etched away using HF at 65°C. The resulting nanowires were removed from the bulk feedstock via sonication in isopropyl alcohol (IPA). The nanowires were stored in IPA.

STEM sample preparation and characterization

The nanowires were drop cast on a lacey carbon on a Cu TEM grid for atomic structure and composition characterization. Liftouts of the MoP and MoP₂ bulk single crystals were made using a Thermo Fisher Scientific Helios G4 UX FIB (Figure S2). Fabrication of the bulk single crystals are described elsewhere. T7,21 STEM, EDX, and 4D STEM data were collected on a Thermo Fisher Scientific Spectra 300 TEM at 300 kV. Simulated structures and diffraction patterns were generated using VESTA, CrystalMaker, and SingleCrystal. 4D STEM data were analyzed using py4D-STEM. In order to determine the Mo:P ratio of the molded nanowires, a k-factor was calculated using EDX data of the MoP and MoP₂ reference crystals.

DFT calculations

The electronic band structure and density of states calculations of bulk Mo₄P₃ were performed from first-principles using Vienna Ab initio Simulation Package (VASP). DFT calculations were performed within the generalized gradient approximation (GGA) as implemented in the Perdew-Burke-Ernzerhof (PBE) functional. We employed an energy cutoff of 600 eV, an electronic momentum k-point mesh of 8 \times 32 \times 4, a Methfessel-Paxton smearing of 0.1 eV, and an energy tolerance of 10^{-8} eV for the total energy convergence, at the calculated bulk lattice parameters of a = 12.482 Å, b = 3.164 Å, and c = 20.495 Å (which are in good agreement with Leclair et al. 24) with the *Pnma* (#62) symmetry, relaxed with a force tolerance of 10^{-3} Å/eV. Vaspkit and Sumo 34 packages were used for analyzing and plotting the band structure.





The predicted conductivity tensor multiplied by the scattering time τ of Mo₄P₃ from ab initio calculations was obtained from Ricci et al.²⁸ We use 1.4 × 10⁻¹⁴ s for τ of MoP²⁹ as a reference, and we estimate τ for Mo₄P₃ to be between 10⁻¹⁴ and 10⁻¹³ s. The resistivity tensors were calculated from these limits (Tables S2 and S3).

Device fabrication and four-point probe measurements

 ${\rm Mo_4P_3}$ nanowires were drop cast onto ${\rm SiO_2/Si}$ substrates and coated with an e-beam resist layer (PMMA 495 A4). Electrode patterns for four-probe measurements were obtained by standard e-beam lithography. 5/50 nm thick Ti/Au electrical contacts were deposited by e-beam evaporation. Resistivity measurements were carried out in vacuum (${\sim}10^{-5}$ torr) at room temperature.

SUPPLEMENTAL INFORMATION

Supplemental information can be found online at https://doi.org/10.1016/j.matt. 2023.03.023.

ACKNOWLEDGMENTS

We thank Sushant Kumar and Ravishankar Sundararaman for helpful discussions on scattering times for Mo_4P_3 . We acknowledge the support of the National Science Foundation Metals and Metallic Nanostructures program for TMNM (DMR 2240956), the Semiconductor Research Corporation for transport measurements (nCORE IMPACT), and the Gordon and Betty Moore Foundation for 4D STEM experiments (EPiQS Synthesis Investigator Award). Q.P.S. acknowledges support from the NSF Graduate Research Fellowship Program. Characterization of the nanowires and DFT calculations were made possible by the Platform for the Accelerated Realization, Analysis, and Discovery of Interface Materials (PARADIM), supported by NSF Cooperative Agreement no. DMR-2039380; the Cornell Center for Materials Research (CCMR) Shared Facilities, supported by the NSF MRSEC program (DMR-1719875); and the Cornell Nanoscale Facility (CNF), supported by NSF grant no. NNCI-2025233. TEM sample preparation was performed on a Helios FIB at the CCMR facilities, supported by NSF (DMR-1539918).

AUTHOR CONTRIBUTIONS

M.T.K., H.J.H., and J.R.S. performed nanomolding; Q.P.S. and J.L.H. performed STEM characterization; B.P. carried out DFT calculations; G.J. performed resistivity measurements; and J.J.C. supervised the project. M.T.K. wrote the manuscript with input from all authors.

DECLARATION OF INTERESTS

The authors declare no competing interests.

Received: November 3, 2022 Revised: February 24, 2023 Accepted: March 20, 2023 Published: April 12, 2023

REFERENCES

- Greer, J.R., Oliver, W.C., and Nix, W.D. (2005). Size dependence of mechanical properties of gold at the micron scale in the absence of strain gradients. Acta Mater. 53, 1821–1830. https:// doi.org/10.1016/J.ACTAMAT.2004.12.031.
- Sohn, S., Jung, Y., Xie, Y., Osuji, C., Schroers, J., and Cha, J.J. (2015). Nanoscale size effects in crystallization of metallic glass nanorods. Nat. Commun. 6, 8157. https://doi.org/10.1038/ ncomms9157.
- Balandin, A.A., Kargar, F., Salguero, T.T., and Lake, R.K. (2022). One-dimensional van der Waals quantum materials. Mater. Today 55, 74–91. https://doi.org/10.1016/J.MATTOD. 2022.03.015.

Matter Article



- Frolov, S.M., Manfra, M.J., and Sau, J.D. (2020). Topological superconductivity in hybrid devices. Nat. Phys. 167, 718–724. https://doi. org/10.1038/s41567-020-0925-6.
- Han, H.J., Liu, P., and Cha, J.J. (2021). 1D topological systems for next-generation electronics. Matter 4, 2596–2598. https://doi. org/10.1016/J.MATT.2021.05.020.
- Li, G., and Felser, C. (2020). Heterogeneous catalysis at the surface of topological materials. Appl. Phys. Lett. 116, 070501. https://doi.org/ 10.1063/1.5143800
- 7. Trimble, C.J., Wei, M.T., Yuan, N.F.Q., Kalantre, S.S., Liu, P., Han, H.J., Han, M.G., Zhu, Y., Cha, J.J., Fu, L., and Williams, J.R. (2021). Josephson detection of time-reversal symmetry broken superconductivity in SnTe nanowires. npj Quantum Mater. 61, 61–66. https://doi.org/10.1038/s41535-021-00359-w.
- 8. Vergniory, M.G., Elcoro, L., Felser, C., Regnault, N., Bernevig, B.A., and Wang, Z. (2019). A complete catalogue of high-quality topological materials. Nature 566, 480–485. https://doi.org/10.1038/s41586-019-0954-4.
- Kiani, M.T., and Cha, J.J. (2022). Nanomolding of topological nanowires. Apl. Mater. 10, 080904. https://doi.org/10.1063/5.0096400.
- Liu, Z., Liu, N., and Schroers, J. (2022). Nanofabrication through molding. Prog. Mater. Sci. 125, 100891. https://doi.org/10.1016/J.PMATSCI.2021.100891.
- Liu, N., Liu, G., Raj, A., Sohn, S., Morales-Acosta, M.D., Liu, J., and Schroers, J. (2021). Unleashing nanofabrication through thermomechanical nanomolding. Sci. Adv. 7, 4567. https://doi.org/10.1126/SCIADV. ABI4567.
- Liu, G., Sohn, S., Liu, N., Raj, A., Schwarz, U.D., and Schroers, J. (2021). Single-crystal nanostructure arrays forming epitaxially through thermomechanical nanomolding. Nano Lett. 21, 10054–10061. https://doi.org/ 10.1021/ACS.NANOLETT.1C03744/ SUPPL_FILE/NL1C03744_SI_001.PDF.
- Liu, Z., Han, G., Sohn, S., Liu, N., and Schroers, J. (2019). Nanomolding of crystalline metals: the smaller the easier. Phys. Rev. Lett. 122, 036101. https://doi.org/10.1103/ PHYSREVLETT.122.036101.
- Liu, N., Xie, Y., Liu, G., Sohn, S., Raj, A., Han, G., Wu, B., Cha, J.J., Liu, Z., and Schroers, J. (2020). General nanomolding of ordered phases. Phys. Rev. Lett. 124, 036102. https://doi.org/10.1103/ PHYSREVLETT.124.036102.
- Khan, M.R., Bu, K., Chai, J.S., and Wang, J.T. (2020). Novel electronic properties of

- monoclinic MP4 (M = Cr, Mo, W) compounds with or without topological nodal line. Sci. Rep. 10, 11502–11509. https://doi.org/10.1038/s41598-020-68349-9.
- Han, H.J., Hynek, D., Wu, Z., Wang, L., Liu, P., Pondick, J.V., Yazdani, S., Woods, J.M., Yarali, M., Xie, Y., et al. (2020). Synthesis and resistivity of topological metal MoP nanostructures. Apl. Mater. 8, 011103. https://doi.org/10.1063/1. 5130159
- Kumar, N., Sun, Y., Xu, N., Manna, K., Yao, M., Süss, V., Leermakers, I., Young, O., Förster, T., Schmidt, M., et al. (2017). Extremely high magnetoresistance and conductivity in the type-II Weyl semimetals WP2 and MoP2. Nat. Commun. 81, 1642–1648. https://doi.org/10. 1038/s41467-017-01758-z.
- Wei, X.-K., Bihlmayer, G., Zhou, X., Feng, W., Kolen'ko, Y.V., Xiong, D., Liu, L., Blügel, S., Dunin-Borkowski, R.E., Wei, X., et al. (2020). Discovery of real-space topological ferroelectricity in metallic transition metal phosphides. Adv. Mater. 32, 2003479. https:// doi.org/10.1002/ADMA.202003479.
- Gall, D., Cha, J.J., Chen, Z., Han, H.J., Hinkle, C., Robinson, J.A., Sundararaman, R., and Torsi, R. (2021). Materials for interconnects. MRS Bull. 46, 959–966. https://doi.org/10.1557/ S43577-021-00192-3.
- Jin, G., Han, H.J., Hart, J.L., Sam, Q.P., Kiani, M.T., Hynek, D.J., Hasse, V., Felser, C., and Cha, J.J. (2022). Vapor phase synthesis of topological semimetal MoP2 nanowires and their resistivity. Appl. Phys. Lett. 121, 113105. https://doi.org/10.1063/5.0106357.
- Kumar, N., Sun, Y., Nicklas, M., Watzman, S.J., Young, O., Leermakers, I., Hornung, J., Klotz, J., Gooth, J., Manna, K., et al. (2019). Extremely high conductivity observed in the triple point topological metal MoP. Nat. Commun. 101, 2475–2477. https://doi.org/10.1038/s41467-019-10126-y.
- Shirotani, I., Kaneko, I., Takaya, M., Sekine, C., and Yagi, T. (2000). Superconductivity of molybdenum phosphides prepared at high pressure. Phys. B Condens. Matter 281–282, 1024–1025. https://doi.org/10.1016/S0921-4526(99)00894-7.
- H. Okamoto, M.E. Schlesinger, and E.M. Mueller, eds. (2016). Alloy Phase Diagrams (ASM International). https://doi.org/10.31399/ asm.hb.v03.9781627081634.
- Leclaire, A., Borel, M.-M., Grandin, A., Raveau, B., and IUCr. (1989). Redetermination of the crystal structure of Mo4P3. Acta Crystallogr. C 45, 540–542. https://doi.org/10.1107/ S0108270188012806.

- Yaws, C.L. (2015). The Yaws Handbook of Vapor Pressure: Antoine Coefficients (Gulf Professional Publishing).
- Clark, P., and Oyama, S.T. (2003). Aluminasupported molybdenum phosphide hydroprocessing catalysts. J. Catal. 218, 78–87. https://doi.org/10.1016/S0021-9517(03) 00086-1.
- Sun, A., Lv, K., Wang, D., and Wu, Z. (2019). Template-free synthesis of porous Mo3P/MoP nanobelts as efficient catalysts for hydrogen generation. Appl. Surf. Sci. 493, 740–746. https://doi.org/10.1016/J.APSUSC.2019. 07.074.
- Ricci, F., Chen, W., Aydemir, U., Snyder, G.J., Rignanese, G.M., Jain, A., and Hautier, G. (2017). An ab initio electronic transport database for inorganic materials. Sci. Data 4, 170085–170113. https://doi.org/10.1038/ sdata.2017.85.
- 29. Han, H.J., Kumar, S., Jin, G., Ji, X., Hart, J.L., Hynek, D.J., Sam, Q.P., Hasse, V., Felser, C., Cahill, D.G., et al. (2023). Topological metal MoP nanowire for interconnect. Adv. Mater. e2208965. https://doi.org/10.1002/adma. 202208965.
- Savitzky, B.H., Zeltmann, S.E., Hughes, L.A., Brown, H.G., Zhao, S., Pelz, P.M., Pekin, T.C., Barnard, E.S., Donohue, J., Rangel Dacosta, L., et al. (2021). py4DSTEM: a software package for four-dimensional scanning transmission electron microscopy data analysis. Microsc. Microanal. 27, 712–743. https://doi.org/10. 1017/S1431927621000477.
- Kresse, G., and Furthmüller, J. (1996). Efficient iterative schemes for ab initio total-energy calculations using a plane-wave basis set. Phys. Rev. B Condens. Matter 54, 11169–11186. https://doi.org/10.1103/PhysRevB.54.11169.
- Perdew, J.P., Burke, K., and Ernzerhof, M. (1996). Generalized gradient approximation made simple. Phys. Rev. Lett. 77, 3865–3868. https://doi.org/10.1103/PhysRevLett.77.3865.
- Wang, V., Xu, N., Liu, J.C., Tang, G., and Geng, W.T. (2021). VASPKIT: a user-friendly interface facilitating high-throughput computing and analysis using VASP code. Comput. Phys. Commun. 267, 108033. https://doi.org/10. 1016/J.CPC.2021.108033.
- M Ganose, A., J Jackson, A., and O Scanlon, D. (2018). sumo: command-line tools for plotting and analysis of periodic *ab initio* calculations.
 J. Open Source Softw. 3, 717. https://doi.org/ 10.21105/JOSS.00717.